EXPERIMENTAL INVESTIGATION OF TURBULENT FLOW IN AN IDEALIZED HUMAN AIRWAY IN THE EXTRATHORACIC REGION

A. Johnstone, A. Heenan, A. Pollard
Department of Mechanical Engineering,
Queen's University
Kingston, Ontario, K7L 3N6 CANADA
andrew@me.queensu.ca, pollard@me.queensu.ca

E. Matida, W.H. Finlay
Department of Mechanical Engineering,
University of Alberta, Edmonton, Alberta
Edmonton, Alberta

ABSTRACT

The mean and RMS axial velocity field in an idealized representation of the human extrathoracic airway (ETA) during steady inspiration was studied experimentally using hot-wire anemometry and flow visualization techniques. Physiologically correct flow rates in the range of 10, 15, 30, 45, 60, and 90 liters per minute for hot-wire measurements and 30, 60, and 120 liters per minute for flow visualization measurements are considered. These data were then compared to previously obtained Particle Image Velocimety (PIV) data and Reynolds-Averaged Navier-Stokes (RANS) Computational Fluid dynamics (CFD), all of which used an identical ETA model. Flow in the ETA was found to be very complex, with separated, secondary, and recirculating flow regions present at numerous model locations. Comparison of hot-wire, PIV and CFD results are made.

INTRODUCTION

In respiratory physiology, knowledge of flow dynamics in the oral airways is essential to the understanding of the deposition of airborne particles. Particles are entrained and transported by inhaled airflow. These flow fields should exert influence upon the deposition patterns of airborne pollutants and pharmacological drugs. Although airflow in the respiratory tract is a complex phenomenon involving numerous physiological processes, it is considered fundamentally to be a fluid mechanical event. Given that the ETA (see figure 1) constitutes approximately one-half of the total length of the respiratory tract, it is interesting to note that much less attention has been paid to this region by the respiratory physiologist.

Although therapeutic aerosols have been carefully engineered to permit maximum transport to the alveolar regions of the lung, in practice typically 80 - 95 % (Gonda, 1992) of the inhaled dose is deposited in the upper airways and channeled to the gastrointestinal tract, which is an unwanted effect. Minimizing upper airway deposition is thus an important issue. For many pharmaceutical inhalation devices, however, deposition in the upper airway is not well understood. Reasons for this lack of understanding include:

- the complex three-dimensional geometry of the ETA, which makes theoretical, numerical and experimental analyses difficult;

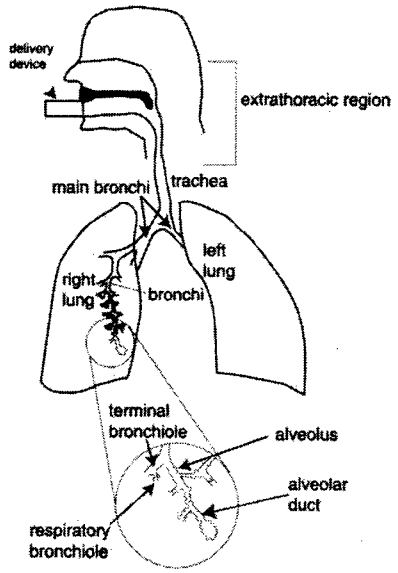

Figure 1: Schematic of human ETA, Finlay 2002.

- the considerable variability in geometry between individuals (Stapleton and Finlay, 1998), as well as between different inhalation devices, which makes general quantitative statements difficult, and
- the presence of transitional or turbulent airflow at flow rates typical of many inhalation devices, partly because such devices commonly produce turbulence internally and partly due to turbulence production within the ETA itself.

The mechanics of ETA particle deposition can be separated into two parts: the flow field generated by the ETA geometry and the interaction of aerosol particles with this flow field. This separation can be seen in more sophisticated ETA deposition predictors, which first model the ETA flow field using computational methods, and then numerically "release" and track the paths of a large number of virtual particles and build up a statistical distribution of their deposition location. The accuracy of these predictions is, of course, dependent on the accuracy of both the CFD and particle dynamics models.

Direct Navier-Stokes simulations of the flow field are precluded due to the extreme computational overhead involved,

and RANS modeling methods are generally used instead. Stapleton et. al. (2000) used k-ε RANS modeling in an idealized representation of the ETA for oral inspiration of polydisperse particles with mean diameter 5 mm. Typically, the accuracy of such deposition predictors is investigated by comparing the results with experimental deposition measurements using gamma scintigraphy, gravimetry, spectroscopy or other techniques. Stapleton et. al. (2000) had good deposition prediction for wholly laminar flow conditions (i.e. flow rate < 2 L/min), but found that significant errors develop at the onset of turbulence. Turbulence will be present during inhalation through drug delivery systems, where flow rates produce Re>2000. Further development is therefore necessary before these methods become a robust tool for predicting deposition under these *in-vivo* conditions. The above-mentioned validation approach does not de-couple errors in the flow-field model from those in the particle dynamics model, which makes it difficult to pinpoint the source(s) of error and their subsequent reduction or elimination. To de-couple the errors it is necessary to make both regional deposition measurements and accurate experimental measurements of the flow field. This paper presents such a survey by comparing hot-wire and flow visualization results with existing PIV and RANS CFD results taken in an identical ETA geometry.

EXPERIMENTAL METHOD

Model Geometry and Manufacture

The geometry of the ETA is rather poorly defined. Not only is there huge inter-subject variability, but its shape also varies with time within a given subject. In the present work experiments were carried out in a physiologically 'averaged' geometrical model of the ETA based on data from computed tomography (CT) scans, magnetic resonance imaging (MRI) scans, direct observation of living subjects and data in the archival literature. Although individual airway models would be useful to study flow patterns in one specific individual, the geometric characteristics of the ETA mentioned above make projection of quantitative results to the general population extremely difficult. The geometry used is built up of simple geometric shapes but possesses all the basic anatomical features of a real ETA. The design is a slight variation of the one described in Stapleton et. al. (2000) and the reader is directed there for the rational behind the geometry and choice of dimensions.

A three-dimensional CAD model of the geometry was designed using the ProEngineer (PTC, Needham, MA) and DeskArtes 3Data Expert (DeskArtes Oy, Helsinki, Finland) software packages. For both hot-wire and flow visualization measurements double-scaled models were used (paying proper attention to dynamic similarity) to permit:

- a reduction in flow velocity, sharper images, and increased spatial and temporal resolution for flow visualizations, and
- sufficient velocity resolution and minimum flow interference to permit precise point-by-point acquisition of data using hot-wire probes.

The models were designed in two halves. Included in the designs were seven hot-wire penetrable ports, slots for laser windows and holes for borescope insertion (for flow visualization measurements), and appendages for bolting the two halves of the model together and for mounting models to the rest of the experimental apparatus. The models were manufactured using a Stratasys FDM8000 rapid-prototyping (RP) system (Stratasys Inc., Eden Prairie, MN). Models generated are made of dry, rigid ABS plastic and are smooth walled. Schroter and Sudlow (1969) have justified utilizing such a model. Flow visualization models were painted matte black to minimize laser reflections. Rubber O-Rings were incorporated around model perimeters along with Dow Corning high vacuum sealant (Dow Corning Corporation, Midland, MI) to prevent any flow leakage through the two mating halves. A nozzle with a 7:1 contraction ratio was used at the model inlet to ensure uniform (ie. plug) inlet conditions at all flow rates.

Experimental Setup

Highly accurate inhalation flow rates through ETA models was achieved using a computer-controlled servomotor-driven pulmonary waveform generator (PWG) system (MH Custom Design, Midvale, Utah). The PWG system delivers 81 microliters of air volume per increment of its DC servomotor's optical rotary encoder, thus giving precise control over flow rates sucked through the model. PWG software tracks and displays flow, volume, and pressure information.

Flow Visualization Apparatus. Seeding of the flow takes place through the use of a smoke wire array system (see figure 2). The hand made device consists of 11 - 0.005" outside diameter stainless steel wires, evenly spaced at 0.1" across the model inlet (i.e. immediately following the inlet nozzle).

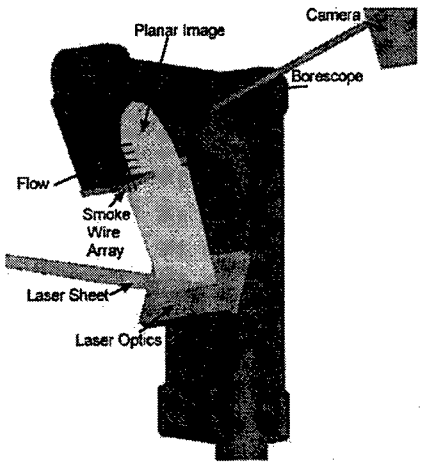

Figure 2: Flow visualization rig set-up (axial plane).

The array is connected to a power source, which supplies the wires with heating current. Light mineral oil is applied to the wires, and when the power source is triggered the wires rapidly heat to burn the oil, generating 11 equally spaced smoke streamlines at the model inlet. The burn time is approximately 1 second. Illumination of the smoke array takes place through use of a Spectra-Physics 5 Watt Ar^+ laser source (Spectra-Physics Inc., Mountain View, CA). The laser beam is adjustable from 0.3 - 3 mm thickness and spread to the appropriate fan angle and focal length using carefully positioned Powell and cylindrical lenses. A multi-element optical system allows positioning of the light sheet in 6 axes. Recording of flow through the model takes place via a Motionscope 1000s CCD high-speed digital imaging system (Redlake Inc., San Diego, CA). The system records sequences of images from 60 to 1000 frames

per second and has a 50 msec adjustable shutter speed. A specially designed borescope is attached to the camera to allow penetration through small holes in the side of the model. In all cases, holes not in use were sealed with wax. Visualizations were taken in both the axial (i.e. cross-sectional) and longitudinal planes at steady inhalation flow rates (of 15, 30, and 120 L/min, physiologically correct) and multiple locations (12 axial, 4 longitudinal) throughout the model. The effect of unsteady acceleration on the fluid mechanics during the early part of inhalation may also be important (Isabey and Chang, 1982), but here we present data only for steady inhalation.

Hot-Wire Apparatus.

Specially designed and custom manufactured 90-degree (boundary layer-type) hot-wire probes (Auspex Corporation, Allentown, PA) were inserted through seven ports along the central sagittal plane of the model at various locations (see figure 3).

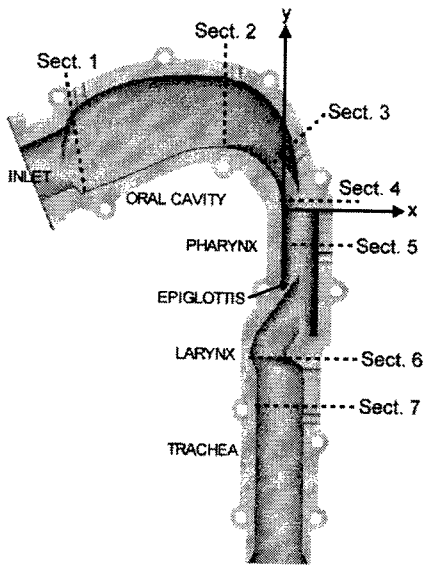

Figure 3: Idealized model geometry showing hot-wire traverse sections with co-ordinate and naming conventions.

Placement of hot-wire insertion depths are controlled to 0.1 mm through the use of a 45 X wide field measuring microscope with reticule (Edmond Scientific Co., Barrington, NJ) and a stepper motor driven traversing mechanism (with 2.5 μm resolution) specially designed to accommodate the model geometry. The microscope is also used to accurately determine model wall distances at each section under which wall proximity effects must be taken into account. As a hot-wire probe is brought in close proximity to a wall (typically less than 2mm in our measurements), the hot-wire signal is affected from the heat-sink effect of the wall. Increasingly higher voltages are recorded as the hot-wire probe is brought closer to the wall with or without flow, so when flow is present higher than actual velocities are recorded. To account for this overestimation, the region and extent to which the hot-wire output voltage is increased with no flow at discrete distances from the model wall is measured. A least squares fit is then applied to these data, and the voltage at each corresponding distance later subtracted from hot-wire measurements in the model at the chosen flow rate.

Precise calibration of hot-wires for in-model measurements also required the construction of a special low-speed calibration system. This consists of the PWG system mentioned above connected by PVC tubing to a calibration rig incorporating a diffuser, rough and fine flow straightening screens, settling chamber and nozzle. As the nozzle exit area is known, a steady PWG exhalation flow rate can be chosen (assuming incompressible flow) to produce the desired reference calibration velocity. Use of the PWG was chosen over conventional fan or compressed calibration air sources for two main reasons:

- Conventional methods require the use of a Pitot-static tube to determine reference velocity. For velocity measurements below approximately 1 m/s (a necessity for this research), however, pitot tubes are hindered by poor sensitivity and the declining accuracy of pressure measurement instrumentation.
- It allows computer-controlled automation of the calibration procedure.

The PWG determined hot-wire calibration velocities will underestimate the actual centerline velocities at the nozzle exit where hot-wire calibration occurs. The nozzle exit velocity profiles will have boundary layers rather than one dimensional plug (i.e. uniform) profile calculated from the PWG. The iterative procedure devised to correct for this effect is:

a) Calibrate the hot-wire assuming plug (i.e. uniform) flow out of the nozzle exit at each velocity (i.e. flow rate).

b) Generate nozzle exit velocity profiles based on the plug flow calibration.

c) For each profile compare measured volume flow rate (i.e. integration of the velocity profile over the nozzle diameter assuming axisymmetric flow) with true flowrate from PWG readout.

d) Correct each velocity by factor (PWG flow / measured flow).

e) Obtain the corrected calibration curve.

f) Repeat steps c) - e) until converged (i.e. the measured flow rate is within 1 % of the PWG flow rate).

RESULTS

Figure 4 presents the PIV velocity magnitude contour plots of Heenan et. al (2003) at 30 L/min. CFD results were obtained using CFX-Tascflow by importing an IGES (Initial Graphics Exchange Specification) file of the identical ETA geometry. The standard k-ω turbulence model (Wilcox, 1998) was utilized with Kato and Launder (1993) modification and near wall treatment for low-Reynolds numbers based on Grotjans and Menter (1992). Endoscopic PIV, as opposed to using standard PIV imaging incorporating a transparent model, was chosen as it is somewhat more established and issues relating to its implementation are better covered in the literature. At full scale U_{inlet} is 0.88, 1.76, and 5.28 m/s for PIV flow rates of 15, 30 and 90 L/min respectively, with corresponding inlet Reynolds numbers, Re_{inlet}, of 1100, 2200, and 6600.

This suggests laminar, transitional, and turbulent flow. Apart for pinpointing some minor structural variations with increasing Re, however, they found streakline plots to be similar for both PIV and CFD results at all three flow rates, suggesting similar flow structure across this range of Reynolds numbers. CFD work appeared to capture well all major separation regions, although recirculation regions were generally slightly larger than those discovered in PIV

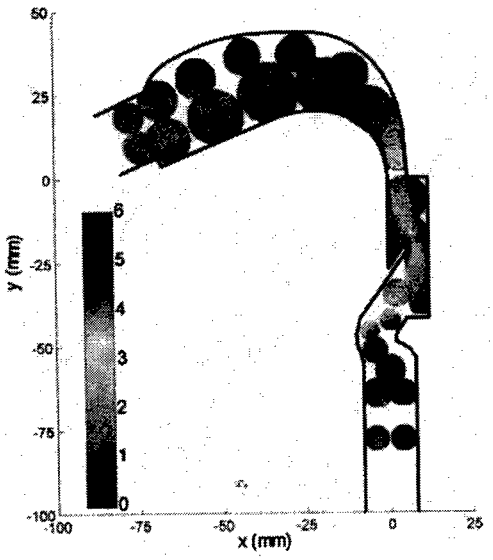

Figure 4: Time-averaged velocity magnitude from PIV with an inhalation flow rate of 30 L/min, normalized by the inlet plug-flow velocity. From Heenan et al. (2003)

experiments. Unexpectedly, they found the primary effect of changing Reynolds number in the PIV experiments to be a significant change in normalized velocity magnitudes. The non-dimensionalized core (akin to centreline) PIV velocities of the 'jets' entering the oral cavity, pharynx and trachea, were found to increase appreciably as *Re* (i.e. the flow rate) was decreased. Worth noting is that this effect was not found to be limited to downstream regions of the model, but was also present to some extent near the inlet. CFD results also show an increase in core velocity but it is very small - about an order of magnitude smaller than seen in the PIV results. This so called Reynolds number effect was also found to be small in the present hot-wire experiments. This discrepancy is best illustrated in the downstream end of the oral cavity where the narrow cross section will accentuate changing viscous effects due to the varying Reynolds number. Figure 5 compares CFD, PIV and hot-wire normalized velocity profiles across the oral cavity contraction section of the model (i.e. traverse section 4 in figure 3). This graph indicates the magnitude of the Reynolds number effect for CFD and hot-wire results is close, but there remains a velocity bias between the two.

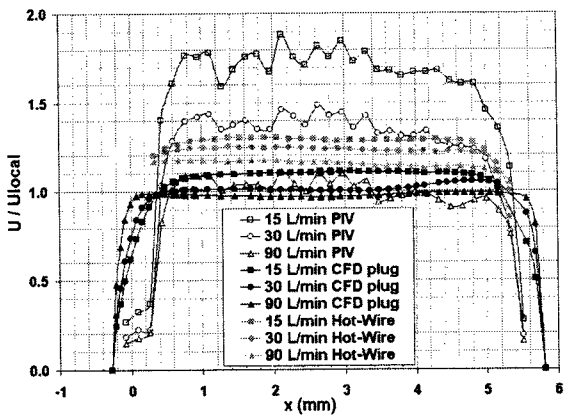

Figure 5: Comparison of velocity magnitude profiles in the oral cavity contraction (model section 4). Profiles have been normalized against the local plug flow velocity.

Heenan et. al. (2003) suggest this large Reynolds number effect, based on the PIV data, indicates that appreciable flow development has occurred prior to the model inlet nozzle in their experiments, and as a result the velocity field boundary condition at the inlet to the oral cavity was not pure plug flow. In their setup, 0.1 m inner diameter (ID) pipe of length 5 L/D was used to connect a flow seeding reservoir to the inlet nozzle (of 7:1 contraction ratio and identical to that used for hot-wire and flow visualization experiments). To determine if this inlet pipe, used exclusively in the PIV work, was a cause for this Reynolds number effect, two actions were taken:

- Hot-wire measurements were taken at the model inlet while incorporating a smooth, 0.1 m ID pipe of length 40 L/D. A longer L/D pipe than that used in the PIV work was chosen to determine, in the limit of fully developed flow, what the effect there would be of the flow condition prior to the inlet nozzle.
- CFD inlet conditions used were inlet plug flows, which employed "top hat profiles" for configurations with and without the inlet nozzle. To allow for possible variations in PIV setup, CFD models were run with three different inlet boundary conditions. The first inlet boundary condition used was plug flow at the inlet to the oral cavity without extension pipe and nozzle. The second was plug flow at the upstream end of the pipe and nozzle arrangement. The third used experimentally measured inlet velocity profiles from the PIV results at the inlet of the oral cavity without pipe and nozzle. In addition, a broad range of different model types were utilized, such as the standard k-ϵ model, Shear Stress Transport (SST) k-ω turbulence model of Menter (1994), Algebraic Stress Model (ASM) of Speziale and Gatski (1993) and Reynolds Stress Model (RSM) of Speziale-Sarkar-Gatski, as incorporated into AEA TASCflow

Hot-wire velocity profiles were measured at all three PIV flow rates with and without the long inlet pipe. It was found, however, that the flow straightening effect of the nozzle suppressed inlet flow deviations to such as degree that differences between the two profiles were negligible. In addition, none of the CFD models or inlet conditions used were found to give any insight into the PIV data that suggested very large viscous effects discussed above. Indeed, major changes in inlet boundary conditions were found to have little effect, suggesting that this difference is intrinsic to the modeling method and not a result of inaccurately defined boundary conditions. This is a significant finding, since Heyerichs and Pollard (1996) found the k-ω turbulence model best for wall bounded flows, especially for cases where there are regions of favorable and adverse pressure gradients, which are present in the flow considered. It is expected that stronger viscous effects present at lower Reynolds numbers should produce a Reynolds number effect as the core fluid velocity increases in order to maintain the overall flow rate, but not to the degree encountered in the PIV measurements.

To help explain the velocity bias discrepancy found between CFD and hot-wire mean velocity magnitudes displayed in figure 5 we consider the flow visualization experiments. Figure 6 presents an instantaneous picture of flow in the axial plane at the oral cavity contraction for a flow rate of 30 L/min. In the flow visualization video from which this snapshot is extracted, fluid close to the central plane of symmetry is observed to flow to the bottom left and right hand

corners of the model and up the walls to the top, producing two equal-sized counter-rotating vortices.

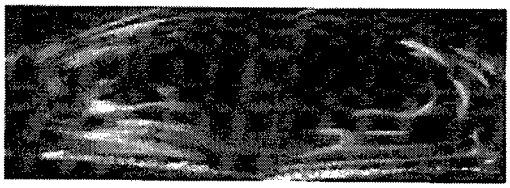

Figure 6: Instantaneous axial flow visualization (30 L/min) at traverse section 4 showing secondary flows caused by model curvature.

These vortices, which act perpendicular to the model longitudinal axis, were observed at all three visualization flow rates. This secondary flow appears to be a Dean flow instability, caused by the strong curvature of the local model geometry (i.e. due to an imbalace of centripetal forces). The Dean number in this region, $\kappa = \left(\frac{\sqrt{A_{local}}}{2R}\right)^{1/2} \frac{Q}{\nu\sqrt{A_{local}}}$ (where A_{local} is the model cross-sectional area), is large (of order 10^3 at 30 L/min) and thus secondary motion is expected to develop soon after the onset of curvature (Berger et. al., 1983). In addition, flow separation is expected as a result of the rapid model curvature. Indeed, separation in this region is confirmed by flow visualizations taken in the longitudinal plane. This separation can result in significantly anisotropic turbulence, which is not captured by any of the RANS models tested in this work. Of significance is that longitudinal flow visualization and PIV results determined the major regions of separated flow to be at the inlet to the oral cavity, see figure 3, (traverse sect. 1), pharynx (i.e. immediately proceeding the oral contraction at sect. 5) and trachea (sect. 7) respectively. Inadequate boundary layer modeling appears to be the main reason for the discrepancy between experiment and CFD. The boundary layers in the present geometry are arguably non-equilibrium and often in the very early stages of development, due to the many regions of separation and reattachment. The flow field at lower Reynolds numbers is likely transitional, which is very difficult to model with available RANS turbulence models.

The secondary motions discovered at the oral cavity contraction are also significant in other respects. Secondary flow is frequently invoked in the respiratory physiology literature due to its direct and indirect role in *e.g.* particle deposition and gas dispersion in airways (Isabey and Chang, 1982). Experimental studies of dispersion in bent tubes by Caro (1966) have shown that secondary flow acts to promote lateral mixing of injected substances such as aerosols. Such mixing, which is observed for substances of low diffusivity and in the absence of turbulence, could actually be very slow without secondary flow. As stated by Pedley et al. (1977), the strength of secondary motions affect the degree of mixing. Most importantly, Lighthill (1972) proposes the pattern of secondary motion observed in steady state could explain why the critical Reynolds number for transition to turbulence increases from 2000 in straight pipes to 6000 for curved pipes. This could be one explanation for the similar flow structure encountered across the range of inlet Reynolds numbers (i.e. of 1100, 2200, and 6600).

Secondary flow was also discovered elsewhere in the model, albeit for different reasons. At the start the oral cavity (i.e. model section 1), flow visualization video shows fluid that begins to move perpendicular to the model longitudinal axis at the left and right-hand sides of the model as in the contraction region discussed above. As inhalation continues, this secondary flow moves down from the sides to the bottom corners of the model and begins to rotate. As a consequence of this flow, a pair of two essentially equal sized counter-rotating vortices are formed at the bottom left and right hand side of the model (see figure 7). We believe this secondary flow is introduced into the flow field, however, by a rapid expansion in model area and attendant flow separation due to the step-like lower geometry of this region, and not because of any rapid changes in model curvature.

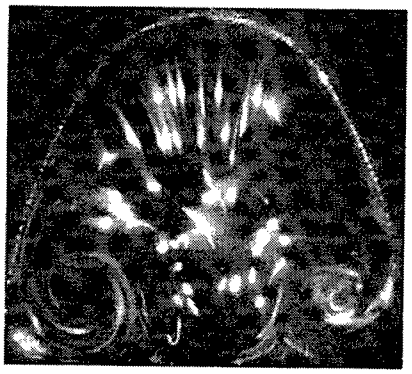

Figure 7: Instantaneous axial flow visualization (30 L/min) at the model inlet (traverse section 1) showing strong secondary flows caused by a rapid increase in model area and separation.

Downstream of the inlet, but still in the oral cavity, hot-wire velcocity profile results indicate the flow accelerates to approximately $1.2U_{local}$ at 90 L/min (see figure 8) due to contraction in cross-sectional area, before passing through the sudden expansion at the start of the pharynx.

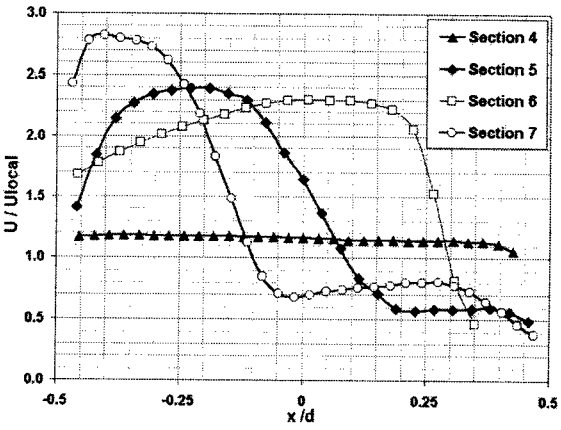

Figure 8: Comparison of velocity profiles at hot-wire traverse sections 4, 5, 6 and 7 at 90 L/min. Profiles have been normalized against the local plug flow velocity and diameter.

The highest velocities in the flow field (corresponding to nearly $3U_{local}$ at 90 L/min), are found at the entrance to the trachea. This acceleration is caused by the small cross-sectional area of the larynx, which is further constricted by a separation 'bubble' formed at the tip of the epiglottis, as observed in flow visualization video. This high-speed flow, which is known as the 'laryngeal jet', enters the trachea at an angle before impinging against and flowing along the anterior wall of the trachea. This induces a highly three-dimensional recirculation region in the posterior half of the trachea.

Not surprisingly, turbulence intensities are lowest at the upstream end of the oral cavity. Overall turbulence intensity

levels in the oral cavity are relatively low. Downstream of the oral cavity there is a significant increase in turbulence intensity levels. The highest turbulence intensities are found in the separated shear layers of the pharynx and trachea (traverse sections 5, 6 and 7 in figure 9).

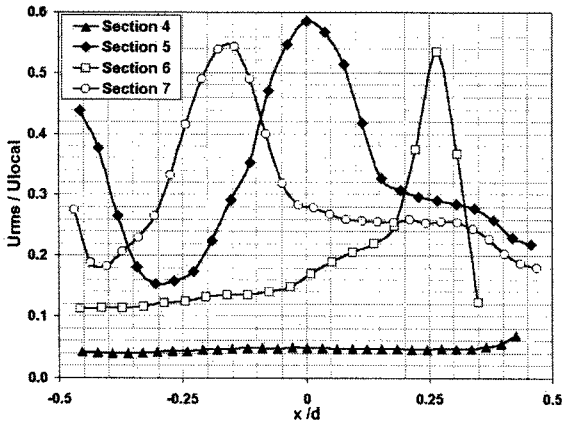

Figure 9: Comparison of turbulence intensities at hot-wire traverse sections 4, 5, 6 and 7 at 90 L/min. RMS velocities have been normalized against the local plug flow velocity and diameter.

With one exception, turbulence intensities at all six flow rates when hot wires were used were found to collapse closely when normailized by the local plug flow velocity, especially at the higher flow rates when the flow is expected to be in the turbulent regime. The only deviation from this trend was encountered at section 5 (i.e. directly downstream of the sudden expansion at the start of the pharynx). This result is not unexpected, as flow visualization results in this region show vortices being shed from the sudden expansion at the pharynx inlet and the presence of the above mentioned recirculation bubble (which appears dependent on flow rate) just upstream of the epiglottis. These two flow features would appear to be an important factor in the change of local turbulence intensity levels with flow rate encountered in this region.

CONCLUSIONS

The mean and turbulence RMS velocities in an idealized representation of the human extrathorasic airway (ETA) were measured experimentally using hot-wire anemometry and flow visualization techniques. These data were compared to previously obtained Particle Image Velocimety (PIV) data and Reynolds-Averaged Navier-Stokes (RANS) Computational Fluid dynamics (CFD). The results illustrate the complex nature of ETA flow, which include several regions of separated, secondary, and recirculating flow. Discrepancies between CFD results (which were obtained using best practice methods) and experimental data have significant ramifications for any subsequent RANS particle deposition modeling. These problems must be addressed before RANS CFD/particle tracking becomes a robust tool for predicting particle deposition in actual *in-vivo* conditions. One option may be to reduce the complexity of the idealized geometry and resulting flow field to see if better RANS modeling can be achieved. However, PIV experiments in real geometries (Heenan et al. 2002) indicate that the complex flow features in this geometry are also present in anatomically correct ETA geometries, and, indeed, the real flow field may be even more complex. Reducing the complexity of an idealized model may seriously compromise its validity as an accurate representation of ETA flow.

ACKNOWLEDGEMENTS

The authors would like to acknowledge the financial support of NSERC. This work has been a result of collaboration between the Aerosol Research Lab., University of Alberta (Finlay) and the Computational and Experimental Fluid Dynamics Lab., Queen's University (Pollard).

REFERENCES

Berger, S. A., Talbot L., and Yao, L. S., (1983), "Flow in curved pipes", *Annu. Rev. Fluid Mech.*, Vol. 159, pp. 461-512.

Gonda E., (1992), Pharmaceutical Inhalation Aerosol Technology, Marcel Dekker, Vol. 54.

Heenan A. F., Grgic B., Pollard. A. and Finlay W. H., (2002), "An investigation of the relationship between the flow field and regional deposition in anatomically realistic extrathoracic airways", submitted to Aerosol Science and Technology.

Heenan A., Matida, E., Pollard, A., Finlay, W. H., "Experimental Measurements and Computational Modeling of flow in an Idealized Extrathoracic Airway", Accepted for publication, Experiments in Fluids, 2003.

Heyerichs, K. and Pollard, A., (1996), "Heat transfer in separated and impinging turbulent flows", *Int. Journal of Heat and Mass Transfer*, Vol. 39, pp. 2385.

Isabey, D., and Chang, H. K., (1982), "A Model study of flow dynamics in human central airways. Part 2: Secondary Flow velocities", *Respiration Physiology*, Vol. 49, pp. 97-113.

Kato, M. and Launder, B. E., (1993), "The modeling of turbulent flow around stationary and vibrating square cylinders", *9th Symp. Turb. Shear Flows*, 10/4/1 to 10/4/6.

Lighthill, M. J., (1972), "Physiological fluid dynamics: A survey", *Journal of Fluid Mechanics*, Vol. 52, pp. 475-497.

Menter, F. R., (1994), "Two-equation eddy-viscosity turbulence models for engineering applications", *AIAA Journal*, Vol. 32, pp. 1598-1605.

Speziale, C. G. and Gatski, T. B., (1993), "Explicit algebraic stress models for complex turbulent flows", *Journal of Fluid Mechanics*, Vol. 254, pp. 59-78.

Stapleton K. W., Guentsch E., Hoskinson M. K. and Finlay. W. H., 2000, "On the suitability of k-e modeling for aerosol deposition in the mouth and throat: a comparison with experiment", *Journal of Aerosol Science*, Vol. 31, pp. 739-749.

Stapleton and Finlay, (1998), "Deposition of Medical Aerosols in the Human Respiratory Tract", Report MA-1, Dept. of Mechanical Engineering, University of Alberta.

Schroter, R. C. and M. F. Sudlow, (1969), "Flow patterns in models of the human bronchial airways", *Respir. Physiology*, Vol. 7, pp. 341-355.

Wilcox D. C., (1998), "Reassessment of the Scale Determining Equation for Advanced Turbulence Models", *AIAA Journal*, Vol. 26, pp. 1299-1310.